Journal of Engineering Science and Technology
Vol. 7, No. 1 (2012) 25 - 40

SOLAR TO AC POWER SOURCE FOR REMOTE AREAS USING SEIG

MEHMET AKBABA*, KHALED AL-RUWAIHI

Department of Computer Engineering, College of Information Technology,
University of Bahrain, P.O. Box 32038, Isa Town, Kingdom of Bahrain
*Corresponding Author: akbabam@itc.uob.bh

Abstract

Photovoltaic generators (PVG) are increasingly used to provide electricity in remote areas. However, in many applications the DC generated electricity by a PVG need to be converted to AC. Traditionally DC to AC inverters have been widely used for this purpose. In this paper, a different system is proposed in which a self excited induction generator (SEIG) driven by a permanent magnet DC motor (DCM) and powered from a PVG through a maximum power point tracker (MPPT) are used. A step-up chopper is utilized as an MPPT unit. The proposed system is modelled in time domain, and a detailed transient and steady-state analysis are presented. The main reason behind analyzing the system in the time domain is because of the fact that for unknown speeds, the methods developed for steady-state analysis of SEIGs can not be applied. The presented work shows that the full available power of the PVG can be harnessed by selecting suitable values for the duty cycle and the frequency of the step up chopper and the excitation capacitor of the SEIG. It is also shown that with such a combination power utilization efficiency of more than 83% can be achieved.

Keywords: AC power, Photovoltaic generators, Remote areas, SEIG, MPPT, Energy efficiency.

1. Introduction

There has been a paradigm shift during the past two decades that promoted new methodology for providing remote areas with electricity. Nowadays, it is an acceptable fact that solar energy has become an important source of electricity which can be used effectively for remote areas [1-2]. However in many applications the DC electricity, which is generated by the PVG, need to be converted to AC. Ideally, the DC-to-AC inverters are the most reliable devices

Nomenclatures

A_{pv}, B_{pv}, C_{pv}	Model parameters of the Akbaba model of PVG *I-V* characteristic
C	SEIG excitation capacitor (per phase), F
f_c	Chopper frequency, Hz
I_{max}	PVG maximum power point current, A
I_{pv}	PVG terminal current, A
I_s	PVG short circuit current, A
i_a	DCM armature winding current, A
i_{cp}	Chopper (MOSFET) current, A
i_L	Load current, A
i_m	Magnetizing current of the SEIG, A
i_{qL}, i_{dL}	*q* and *d* axis components of the load current, A
i_{qr} , i_{dr}	Rotor *q* and *d* axis currents respectively, A
i_{qs}, i_{ds}	Stator *q* and *d* axis currents respectively, A
J_{tot}	Total inertia of the drive shaft, kgm^2
k_m	DCM torque constant, Nm/A
L	Load inductance (per phase), H
L_a	Inductance of the DCM armature winding, H
L_{cp}	Inductance of the chopper coil, H
L_r, L_s	Rotor and stator windings self-inductances, respectively, H
M	Mutual inductance between SEIG stator and rotor windings, H
P_{loss}	Total system power losses = P_{pv} - P_{out} , W
P_{max}	Maximum available PVG power, W
P_{msmt}	Mismatch power = P_{max} - P_{pv} , W
P_o	Number of pole pairs of the SEIG
P_{out}	System output power (load power), W
P_{max}	PVG maximum power point power, W
P_{pv}	PVG power, W
R	Load resistance (per phase), Ω
R_a	Inductance of the DCM armature winding, Ω
R_{cp}	Resistance of the chopper coil, Ω
R_r, R_s	Rotor and stator windings resistances respectively, Ω
V_a	DCM armature winding voltage, V
V_{dr}, V_{qr}	Rotor *d* and *q* axis voltages respectively , V
V_{ds}, V_{qs}	Stator *d* and *q* axis voltages respectively, V
V_{max}	PVG maximum power point voltage, V
V_{oc}	PVG open circuit voltage, V
V_{pv}	PVG terminal voltage, V

Greek Symbols

δ	Copper duty cycle
η	Power utilization efficiency=P_{out}/P_{max}
λ_{qr}, λ_{dr}	Rotor *q* and *d* axis flux linkages respectively, Wb-turns
λ_{qs}, λ_{ds}	Stator *q* and *d* axis flux linkages respectively, Wb-turns
ω_r	Shaft speed, rad/s

used for this purpose. On the other hand induction motors used in remote areas are often purchased for certain task, and they are kept idle upon completion of

that task. Hence, these motors, with addition of a step-up copper can be utilized to convert solar energy into AC electricity.

The purpose of this paper is to study the feasibility of such a system by providing a detailed transient and steady-state analysis. The proposed system is an improved version of the system proposed by Alghuwainem [3], which composed of a DCM directly coupled to a PVG which is used to drive a SEIG to obtain an AC power source. It is believed that the original system [3] needed further development due to the following drawbacks:

- The DCM was directly coupled to the PVG without involving an MPPT unit. As was already mentioned by Alghuwainem [3], without an MPPT unit it was impossible to harness the full available power of the PVG unless a DCM-load unit is selected such that the resulting *I-V* characteristic of the DCM offers natural match to the I-V characteristic of the PVG. Moreover, even with such predetermined selection, the full available power of the PVG can be harnessed only at a certain solar radiation level (e.g., at a 100% solar radiation), as can be observed from the resulted analysis [3]. As the solar radiation level drifts away from 100% the mismatch power grows more and more.
- Only the steady-state analysis was considered. In transient operation, the behaviour of the SEIG shows significant variations than its steady-state operation. In addition, when driving the SEIG with a variable speed prime mover, i.e., when starting from rest and then loading it after a sufficient voltage build-up, voltage collapse may takes place if the excitation capacitor was not carefully selected. As will be explained later, the minimum required capacitance calculated based on the steady-state theory of operation [4-7] can't be applied because the speed is unknown, whereas all known methods available for steady-state analyses of SEIGs assume that the speed is known.
- Only the PVG power, which is the input power to the DCM, was considered. The output power and the power utilization efficiency (η) have been neglected. It will be shown later that under constant load (fixed R and L) and duty cycle, the system input power (P_{pv}) drops slowly as the value of the capacitor increases, whereas the system output power drops sharply (and that η drops sharply too).
- Only a resistive load was considered, while the time constant of an inductive load (L/R), or in another word the load power factor, has a very significant effect on the behaviour of the SEIG.

In this research work, the above mentioned drawbacks of the system proposed in [3] are taken into considerations and are overcome.

In the past, several applications have utilized DC-DC step up choppers as MPPT units [8-10]. Saied et al. [8] used a DC-DC step up chopper as an exact analogy to an ideal transformer, in which only the voltage ratio was considered. In other applications [9-10], only the steady-state transfer function of the DC-DC step up choppers was utilized, whereas the function is not valid for transient operation. In this work, a detailed time domain analysis of the DC-DC step up chopper under investigation is used. Moreover, the MPPT unit used in this paper is an improved version of the MPPT unit used in earlier publications [8-10]. Improvements are achieved by including two filter capacitors (C_1 and C_2), which

have improved the stability of the overall system, by reducing the ripple in the PVG voltage and the input voltage of the DCM.

In the literature, the operating principles and performance analysis of the SEIGs have been subject to extensive research. An exhaustive list of references is given in Bansal [11]. A major drawback of the SEIGs is the variations in output voltage and frequency with different loads. Nonetheless, several researchers have devoted efforts to overcome this drawback [12-18]. Yet in many applications implemented in remote areas, regulation of the output voltage and frequency are considered to be of a secondary importance. For this reason, this topic is not being addressed in this paper.

The system under investigation in this research work has been modelled in real time in order to predict both the transient as well as the steady-state performance within the same simulation program. By taking a model example system, detailed performance analyses is presented which can be used as a convenient tool for scaling the system components before installing an actual system. In this paper it is also shown that a power utilization efficiency of more than 83% can be achieved. It is known that this level of efficiency is considered to be reasonable for such systems.

2. Mathematical Model of the System under Investigation

The block diagram of the system under investigation in this paper is shown in Fig. 1. The system composes of a PVG, a matching circuit as a maximum power point tracking unit (MPPT), a permanent magnet DC motor (DCM), a SEIG and an AC load which is a series connected *R-L* circuit. The circuit diagram of the MPPT unit is given in Fig. 2.

The voltage equations of the SEIG [19], excitation capacitor and AC load combination are given below, in *q-d* stationary reference frame. All currents, voltages and flux linkages are referred to the stator side of the SEIG.

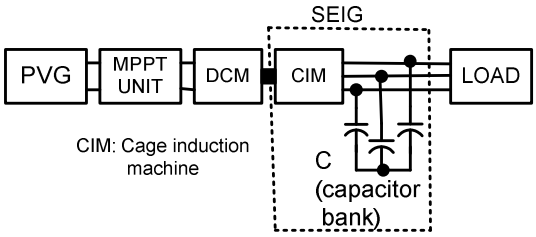

Fig. 1. Block Diagram of the Proposed System.

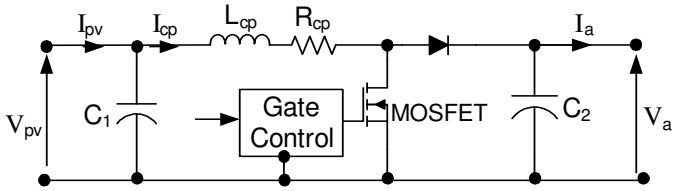

Fig. 2. Circuit Diagram of the MPPT Unit.

$$\begin{bmatrix} V_{qs} \\ V_{ds} \\ V_{qr} \\ V_{dr} \end{bmatrix} = \begin{bmatrix} -(R_s + L_s p) & 0 & Mp & 0 \\ 0 & -(R_s + L_s p) & 0 & Mp \\ -Mp & P_o \omega_r M & R_r + L_r p & -P_o \omega_r L_r \\ -P_o \omega_r M & -Mp & P_o \omega_r L_r & R_r + L_r p \end{bmatrix} \begin{bmatrix} i_{qs} \\ i_{ds} \\ i_{qr} \\ i_{dr} \end{bmatrix} \quad (1)$$

where $p=d/dt$ (differential operator)

$$\frac{dV_{qs}}{dt} = \frac{i_{qs} - i_{qL}}{C} \quad (2)$$

$$\frac{dV_{ds}}{dt} = \frac{i_{ds} - i_{dL}}{C} \quad (3)$$

$$\frac{di_{qL}}{dt} = \frac{V_{qs} - R\, i_{qL}}{L} \quad (4)$$

$$\frac{di_{dL}}{dt} = \frac{V_{ds} - R\, i_{dL}}{L} \quad (5)$$

The current-voltage characteristic of the PVG is modelled using Akbaba model [20], which is given as:

$$i_{pv} = \frac{V_{oc} - V_{pv}}{A_{pv} + B_{pc} V_{pv}^2 - C_{pv} V_{pv}} \quad (6)$$

The complete details and determination of the parameters of the Akbaba model used in Eq. (6) in addition to the details of the PVG being used in this investigation can be found in Akbaba [20]. The PVG output power is given as:

$$P_{pv} = V_{pv} I_{pv} \quad (7)$$

The maximum power point voltage of the PVG, V_{max}, is expressed as [20]:

$$V_{\max} = \frac{V_{oc}\left(1 - \sqrt{1 - I_{sc}\left(C_{pv} - B_{pv} V_{oc}\right)}\right)}{I_{sc}\left(C_{pv} - B_{pv} V_{oc}\right)} \quad (8)$$

The maximum power point current, I_{max}, can be obtained by substituting Eq. (8) into Eq. (6), and hence the maximum available power of the PVG, P_{max}, is obtained by substituting V_{max} and I_{max} into Eq. (7).

The equations governing the operating behaviour of the MPPT unit are given in the following section. Since the MPPT includes a MOSFET chopper, then two sets of equations will be given; one set for the chopper *on* period and the other for the chopper *off* period.

When the chopper MOSFET is *on* the PVG output voltage is:

$$V_{pv} = R_{cp} i_{cp} + L_{cp} \frac{di_{cp}}{dt} \quad (9)$$

$$\frac{dV_{pv}}{dt} = \frac{i_{pv} - i_{cp}}{C_1} \quad (10)$$

When the chopper MOSFET is *off* the PVG output voltage is:

$$V_{pv} = R_{cp} i_{cp} + L_{cp} \frac{di_{cp}}{dt} + V_a \tag{11}$$

$$\frac{dV_{pv}}{dt} = \frac{i_{pv} - i_{cp}}{C_1} \tag{12}$$

$$i_{cp} = i_a + C_2 \frac{dV_a}{dt} \tag{13}$$

The equation for the armature voltage of the DCM is given by:

$$V_a = R_a i_a + L_a \frac{di_a}{dt} + k_m \omega_r \tag{14}$$

Finally, the equation for the motion of the shaft connecting the DCM to the SEIG is:

$$J_{tot} \frac{P_o \, d\omega_r}{dt} = k_m \, i_a - \frac{3}{2} M \left(i_{ds} \, i_{qr} - i_{qs} \, i_{dr} \right) \tag{15}$$

The output power is computed as:

$$P_{out} = 3RI_L^2 \tag{16}$$

where I_L is the rms value of the load current and it is obtained as:

$$I_L = \sqrt{\left(i_{dL}^2 + i_{qL}^2 \right) / 2} \tag{17}$$

The instantaneous amplitude of the magnetizing current is required for obtaining the saturated magnetizing inductance M of the SEIG, which is computed as:

$$i_m = \sqrt{\left(i_{qs} - i_{qr} \right)^2 + \left(i_{ds} - i_{dr} \right)^2} \tag{18}$$

The resulting differential equations of the system are solved using *Runge-Kutta* fourth order method [21]. A computation step size of 5.3333×10^{-5} seconds is adopted. This step size is chosen in order to have five solutions for the *on* period of the MPPT chopper, at a chopper frequency f_c = 1.2 kHz.

3. Application Example and Discussions of the Results

Is it is well known that the initial installation costs of a PVG is considerably high. Therefore it should be operated on its maximum power trajectory, i.e., system should be tuned in such a way that the PVG delivers its maximum available output power P_{max}. To ensure achieving this condition, an MPPT unit is required to perform the required matching between the PVG and the load. In this investigation a step up DC-DC converter is used as an MPPT unit, as shown in Fig. 2. The unit contains a MOSFET chopper with a PWM pulse control. Two filter capacitors (C_1 and C_2) are added in order to stabilize the PVG and the DCM voltages during transients.

To ensure operating the PVG around its maximum power trajectory, the following two requirements need to be satisfied:

i. An optimum duty cycle and frequency pair must be identified for the MPPT unit [22]. This duty cycle and frequency pair is load dependent, i.e., when load changes the optimum duty cycle-frequency pair has to be updated [22]. To simplify this process, the chopper frequency in this investigation was kept constant at f_c=1.2 kHz, while the optimum duty cycle has been identified independently for each load. For a load of R=27 Ω and L=30 mH (with an excitation capacitor value corresponding to a 2 p.u. capacitive reactance), the optimum duty cycle is obtained as δ=0.3 (30%). It should be noted that the optimum value of the duty cycle results in maximum PVG power and it is independent of the optimum value of the SEIG excitation capacitor. Optimum value of the excitation capacitor is required for maximum SEIG output power.

ii. Optimum value of the SEIG excitation capacitor must be identified. In this investigation the optimum value of the excitation capacitor is identified by utilizing the following steps:

Step 1: Using a p.u. speed of 0.95 and a magnetizing inductance equals to 92% of its unsaturated value in the method described in [6] find the maximum value of the frequency (F_{max}) of the voltage generated by the SEIG.

Step 2: Utilizing F_{max} in the method described in [6], find the minimum required capacitance C_{min}.

Step 3: Use C_{min} as excitation capacitor in the transient program and find the steady-state speed.

Step 4: Using the steady-state speed (p.u. value) obtained in part (c) repeat the steps (a) and (b). The value of C_{min} obtained in this case is almost the optimum capacitance value that results in almost the best P_{pv} and P_{out}. Note that further iterations will not improve the results. Applying the above procedure for a load of $R = 27\ \Omega$ and $L = 30$ mH, the first attempt resulted in a frequency $F_{max} = 0.8871$ p.u. which is equal to 53.22 Hz and C_{min} = 99.65 μF. Using this value of C_{min} as an excitation capacitor in the transient program, the steady-state speed was obtained to be equal to 0.8925 p.u. Finally using this value of the speed in the method given in [6] resulted in F_{max} = 0.786 p.u. which is equal to 47.16 Hz and C_{min} = 114.24 μF ≈ 114 μF. This value of the capacitor is accepted as the optimum capacitor value and used for obtaining the results presented in the following section. It will be shown that this value of excitation capacitor gives excellent results.

The results presented in the following section are computed using $f_c = 1.2$ kHz, $\delta = 0.3$ and $C = 114$ μF, for a load of $R = 27\ \Omega$ and $L = 30$ mH. The starting sequence of the system under study was established as follows:

- During the first 350 ms, the DCM allowed to speed up freely with no load and without excitation capacitors being connected across the SEIG.

- At t=350 ms, a bank of excitation capacitors is switched on to the SEIG, but still without a load. Hence the SEIG is allowed to build up voltage without experiencing voltage collapse.
- Finally the load is connected to the SEIG at t=800 ms.

The magnetizing inductance of the SEIG is modelled in terms of magnetizing current i_m as:

$$M = 0.2476 \text{ H} \quad \text{for} \quad i_m \leq 0.846 \text{ A} \tag{19}$$

and, for $i_m > 0.846$ A:

$$M = a_1 i_m^5 + a_2 i_m^4 + a_3 i_m^3 + a_4 i_m^2 + a_5 i_m + a_6 \tag{20}$$

The coefficients appearing in Eq. (20) are obtained using curve fitting process and their values were obtained as follow:

$a_1 = -5.6016\times10^{-7}$, $a_2 = 37.521\times10^{-6}$, $a_3 = -10.462\times10^{-4}$,

$a_4 = 14.0451\times10^{-3}$, $a_5 = -9.3757\times10^{-2}$, $a_6 = 29.49354\times10^{-2}$.

The current-time characteristic of the PVG is illustrated in Fig. 3. As can be depicted from this figure, at steady-state operation the PVG current converges to a value very close to the maximum power point current, I_{max}. This is a clear indication to the fact that the PVG output power converges to a value very close to its maximum available output power, P_{max}. Furthermore, the voltage-time characteristic of the PVG is illustrated in Fig. 4. This Figure shows also the output voltage of the MPPT, which is the input voltage to the DCM. By analyzing the voltage-time characteristic it can be concluded that the role of the MPPT unit is obvious. It steps up the PVG voltage to a reasonable value at which the motor absorbs maximum power from the PVG and hence obtain the best possible efficiency. It is also evident from Fig. 4 that at steady-state operation the PVG voltage converges to a value very close to its maximum power trajectory voltage, V_{max}, which is another indication to the fact that the PVG operates almost at its maximum available power, P_{max}.

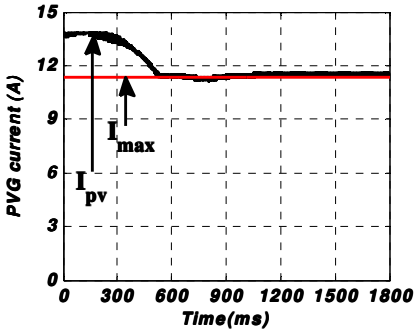

Fig. 3. Current-Time Characteristics of PVG (δ=0.32, f_c=1.2 kHz, R=27 Ω, L=30 mH).

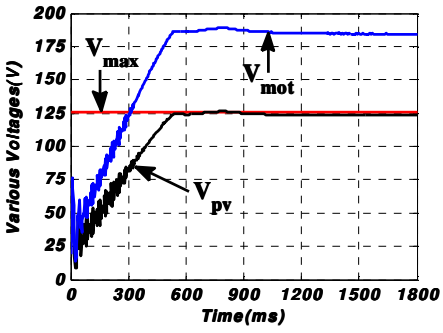

Fig. 4. PVG and DCM Voltages versus Time (δ=0.32, f_c=1.2 kHz, R=27 Ω, L=30 mH).

It worth mentioning that all of the results presented in this paper are given for a 100% solar radiation which is assumed to corresponds to a solar radiation of 1000 W/m2, which gives $I_{max} = 11.327$ A, $V_{max} = 125.62$ V and $P_{max} = 1422$ W.

In Fig. 5, variations of the transient SEIG terminal voltage, SEIG stator current, capacitor current and load current versus time are shown (for $f_c = 1.2$ kHz, $\delta = 0.3$ and $C = 114$ μF, $R = 27$ Ω and $L = 30$ mH). This figure shows that with a suitable value of excitation capacitor and sufficient speed, the SEIG smoothly builds up its voltage. In addition, once the load is connected (at $t = 850$ ms) there is a significant drop in the SEIG terminal voltage. From the magnified version of Fig. 5(a), it can be seen that there is also a significant reduction in the frequency of the SEIG voltage. The level of reduction in the frequency is less than the drop in the terminal voltage. Thus it can be observed from Figs. 5(b) and 5(c) that while SEIG is unloaded (until $t = 800$ ms) the SEIG stator current and the capacitor current are equal. Following the connection of the load, the rates of reduction in the SEIG and capacitor currents are different. This difference is due to the fact that when the load is connected the capacitor should supply both the magnetizing current of the SEIG and the reactive component of the load current. Trends of various signals demonstrated in Fig. 5 confirm the validity of the mathematical modelling presented in the previous section.

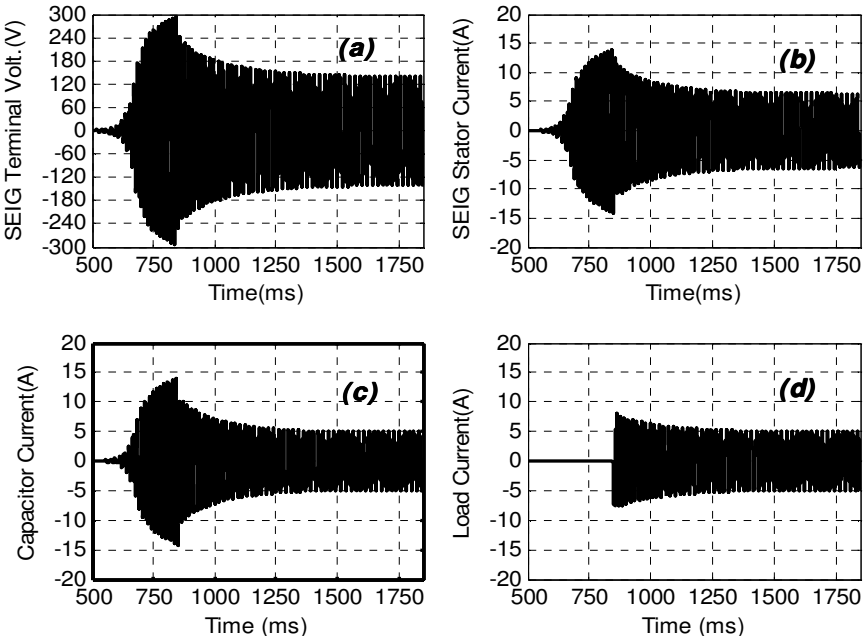

Fig. 5. SEIG Terminal Voltage (a), SEIG Stator Current (b), Capacitor Current (c) and Load Current (d) versus Time (δ=0.41, f_c=1.2 kHz, R=25 Ω, L=30 mH, C=114 μF).

The system input power (P_{pv}) computed using Eq. (7), and the output power (P_{out}) computed using Eq. (16) are illustrated in Fig. 6 (for f_c=1.2 kHz, δ=0.3 and C=114 μF, R=27Ω and L=30 mH). For comparison purposes, Fig. 6 also shows the maximum available power of the PVG, P_{max}. It can be observed from this figure that

at steady-state operation P_{pv} converges to 1420.4 W which is very close to P_{max}, while P_{out} converges to 1184.7 W. This means that the power utilization efficiency of 1184.7/1422 = 0.833 (83%) is achieved. Also at steady-state operation the mismatch power is P_{msmt}=1422-1420.4 = 1.6 W, which is only 0.11% of P_{max}. This proves that the MPPT unit, with correctly selected values of duty cycle and chopping frequency pair, serves as an excellent load matching unit and enables the PVG to deliver its maximum power.

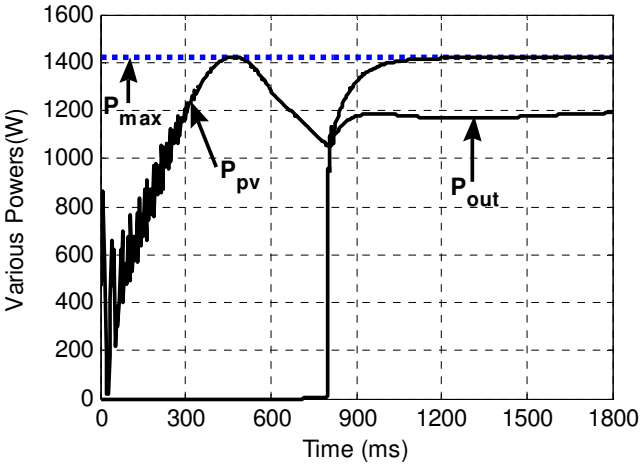

Fig. 6. P_{pv}=P_{in} and P_{out} versus Time (δ=0.3, f_c =1.2 kHz, R=27 Ω, L=30 mH, C=114 μF).

It is also important to study the effects of the load power factor on the system performance. In order to achieve that, the steady-state values of P_{pv}, P_{out}, P_{loss} and overall efficiency are computed by holding the value of the load resistance constant at R = 27 Ω and varying the value of the load inductance in the range from 0 to 240 mH in steps of 5 mH (for δ = 0.30, f_c = 1.2 kHz and C = 114 μF). The results of this analysis are illustrated in Figs. 7 to 9 respectively.

The variations of P_{pv}, P_{out} and P_{loss} versus the load power factor at a rated frequency are illustrated in Fig. 7. It can be observed from this figure that at low values of the power factor, the value of P_{loss} is very large and it improves as the power factor increases. This is due to large SEIG current at low power factors, which results in high joule losses in the SEIG windings. This argument is further verified by Fig. 8. It can be seen therein that as the power factor increases the *rms* SEIG current drops sharply. On the other hand, the load current shows a steady increase as the power factor increases (Fig. 8). This relative trend between the load current and the SEIG current also implies that the capacitor and the magnetizing currents are decreasing as the power factor increases. The power utilization efficiency versus the power factor is illustrated in Fig. 9. One of the important conclusions which can be observed in this figure is that for the power factor values ranging from 0.7 to 1.0 the capacitor value and the duty cycle can be held constant if a drop of around 5% in power utilization efficiency can be tolerated. This property may be considered as an important advantage as in many practical applications the load power factor is above 0.7. This property will also results in economical benefit by requiring only a single value of the capacitor for a range of operating conditions.

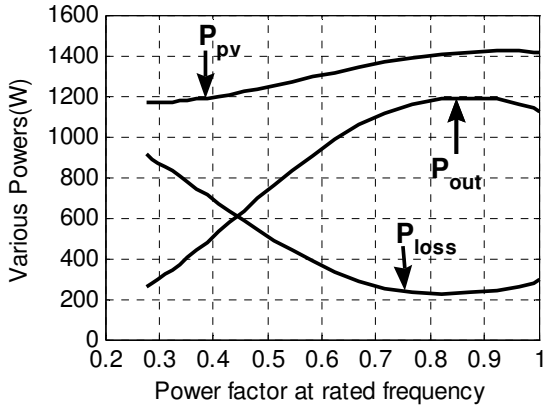

Fig. 7. P_{pv}, P_{out} and P_{loss} versus Power Factor at Rated Frequency (δ=0.3, f_c=1.2 kHz, C=114 µF, R=27 Ω, L=0,…,240 mH).

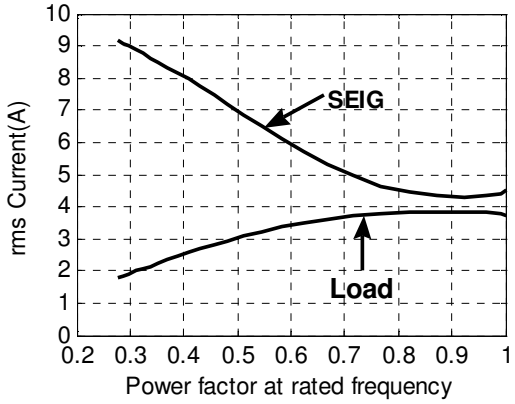

Fig. 8. rms SEIG and Load Currents versus Power Factor at Rated Frequency (δ=0.3, f_c=1.2 kHz, C=114 µF, R=27 Ω, L=0,…,240 mH).

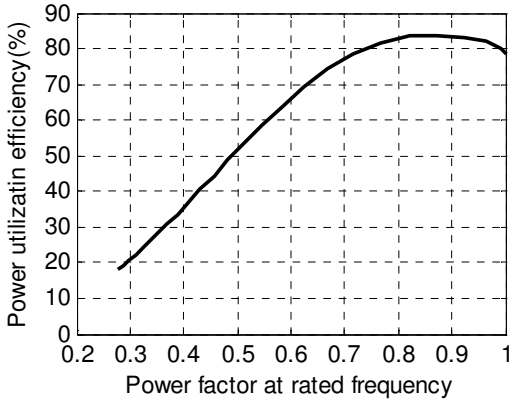

Fig. 9. Power Utilization Efficiency (P_{out}/P_{max}) versus Power Factor at Rated Frequency (δ=0.3, f_c=1.2 kHz, C=114 µF, R=27 Ω, L=0,…,240 mH).

In [3] only P_{pv} is analyzed and it is shown that moderate variations take place in P_{pv} when C varies from1.5 p.u. to 2.p.u. Analysis of P_{out} and the energy utilization efficiency are not considered. It will be shown below that regarding P_{pv} the argument raised in [3] is partially true if the value of C does not vary widely when the load varies within large limits. However, this argument is not true for P_{out} and the power utilization efficiency. To clarify this claim, the steady-state values of P_{pv}, P_{out}, power utilization efficiency, P_{msmt} and P_{loss} are computed for values of C varying in the range from 80 μF to 220 μF in steps of 5 μF, with $R = 24\ \Omega$, $L = 40$ mH, f_c=1.2 kHz, and $\delta = 0.30$. The results are demonstrated in Figs. 10 to 12. It can be seen from Fig. 10 that while the capacitor value remains in the range from 95 μF to 175 μF the maximum deviation in P_{pv} is approximately 3.8%. The corresponding maximum deviation in P_{out} is more than 10%. It can be seen from the same figure that for $C = 95$ μF and $C = 175$ μF the PVG powers are almost the same (1366.5 W and 1366.3 W). On the other hand at $C = 95$ μF P_{out} is 1216.8 W and at $C = 175$ μF, P_{out} is 1096.2 W. It follows from these results that the power utilization efficiency at $C = 95$ μF is 1216.8/1422 = 85.6%, while at $C = 175$ μF it is 1096.2/1422 = 77%. Hence, it is clear from these results that the selection of an optimum capacitance value requires a detailed study of P_{pv}, P_{out} and P_{msmt} all together. Thus considering only P_{pv} is not sufficient for obtaining high power utilization efficiency.

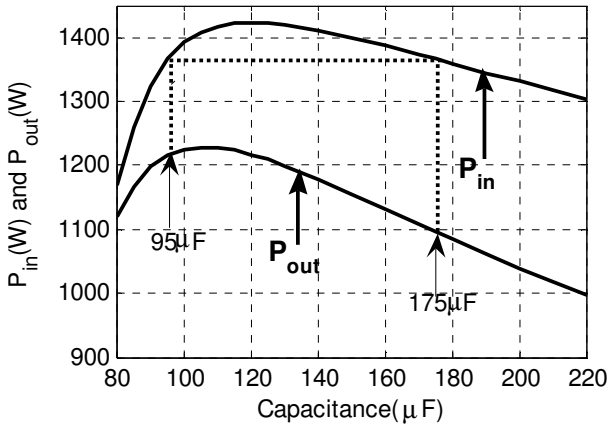

Fig. 10. P_{in}=P_{pv} and P_{out} versus Capacitance (δ=0.3, f_c=1.2 kHz, R=24 Ω, L=40 mH).

Figure 11 shows that the power utilization efficiency remains more than 80% when the capacitor value varies in the range from C=90 μF to C=150 μF. It can be observed from Fig. 12 that power losses are increasing when increasing the value of C. Also it is clear from the same figure that for values of C greater than 120 μF the P_{msmt} is increasing with increasing values of C. For values of C greater than 150 μF, the power utilization efficiency decreases almost linearly with the increasing value of C (Fig. 11). This is due to increased joule losses of the SEIG windings at large values of C. Furthermore, the maximum power utilization efficiency is obtained when the capacitor value is around C=105 μF. It can be concluded from this analysis that ideally the chopper duty cycle should be adjusted such that P_{msmt} is a

minimum at the minimum possible capacitor value, at which the SEIG voltage will not collapse when moderate load and speed variations take place.

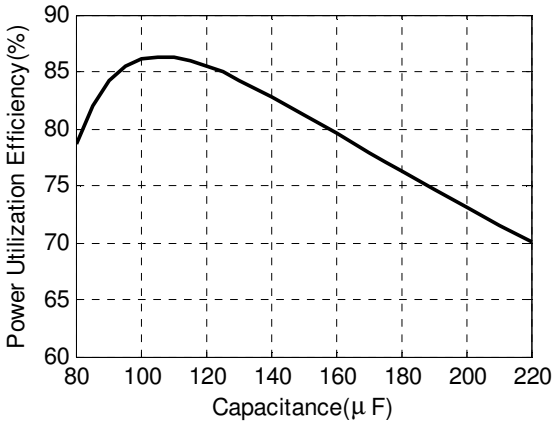

Fig. 11. Power Utilization Efficiency (P_{out}/P_{max}) versus Capacitance (δ=0.3, f_c=1.2 kHz, R=24 Ω, L=40 mH).

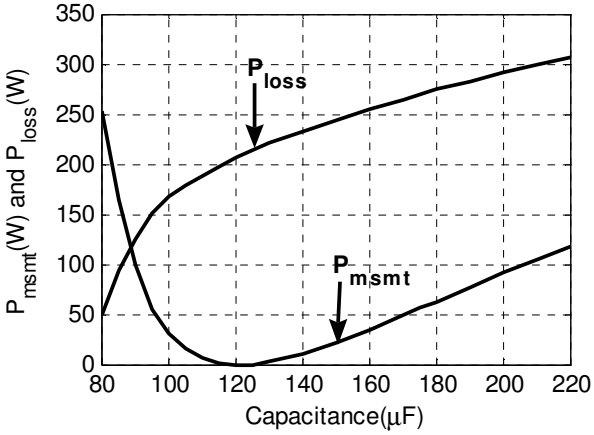

Fig. 12. P_{msmt} and P_{loss} versus Capacitance (δ=0.3, f_c=1.2 kHz, R=24 Ω, L=40 mH).

It was mentioned above that to maximize the power utilization efficiency the duty cycle must be optimized at lowest possible capacitor value, which means minimization of the joule losses in the SEIG. To clarify this argument a search was conducted to obtain the optimum duty cycle for a capacitor value of C=90 μF, with the same load values used to obtain Figs. 10 to 12. It was found that the optimum duty cycle for this case is δ=0.41. Figure 13 shows P_{pv} and P_{out} versus time characteristics obtained with this duty cycle. It can be observed from this figure that the mismatch power in this case is only 0.2 W, which is a negligible figure. At steady-state operation, P_{out} converges to 1295.1 W, which yields a power utilization efficiency of 1295.1/1422=91%. Thus it can be concluded from these results that the mismatch error can be eliminated and the power utilization efficiency can be maximized by identifying matching values for C, δ and f_c.

Values of the parameters used for system components are given in *Appendix A*.

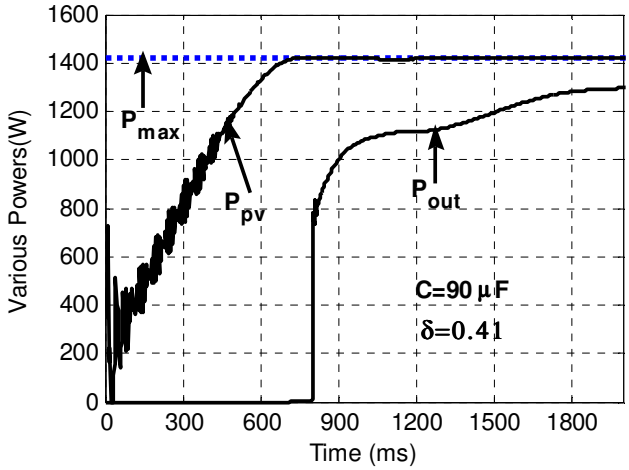

Fig. 13. P_{pv} and P_{out} versus Time (δ=0.41, f_c=1.2 kHz, R=24 Ω, L=40 mH, C=90 µF).

4. Conclusions

This paper presented a detailed transient and steady-state analysis of a system that can be used for converting the PVG power into AC power suitable for applications in remote areas. The proposed work is an alternative system, which could be used when power conditioning units built around DC-to-AC inverters are not available. The proposed system is composed of a SEIG driven by a DCM which is powered from a PVG through an MPPT unit. The following conclusion may be drawn from this investigation:

- Since the speed is not known, the methods developed for steady-state analysis of SEIGs can not be applied directly. Therefore to obtain reliable results the system has to be modelled in time domain.
- To maximize the power utilization efficiency, an MPPT unit has to be incorporated instead of direct coupling the DCM to the PVG.
- The value of the excitation capacitor C has significant effect on the power utilization efficiency. The power utilization efficiency decreases with increasing values of excitation capacitor C. This is due to the fact that the joule losses in the SEIG windings are increasing with the increasing values of C. To obtain maximum power utilization efficiency under a certain load, it is recommended that the value of the duty cycle and f_c have to be matched to a minimum possible value of C, so that the SEIG will not be driven into voltage collapse when moderate variations take place in the load and the speed.
- The load power factor has significant effects on the power utilization efficiency. Therefore when the load changes the duty cycle has to be modified accordingly.
- Using the proposed system, it is possible to obtain a power utilization efficiency of 83% or more.

References

1. Asano, H.; Yajima, K.; and Kaya, Y. (1996). Influence of photovoltaic power generation on required capacity for load frequency control. *IEEE Transactions on Energy Conversion*, 11(1), 188-193.
2. Kuo, Q.; Klein, S.A.; and Beckman, W.A. (1998). A method for estimating the long-term performance of a direct-coupled PV pumping system. *Solar Energy*, 64(1-3), 33-40.
3. Alghuwainem, S.M. (1996). Performance analysis of a PV powered DC motor driving a 3-phase self-excited induction generator. *IEEE Transactions on Energy Conversion*, 11(1), 155-161.
4. Malik, N.H.; and Al-Bahran, A.H. (1990). Influence of terminal capacitor on the performance characteristic of a self excited induction generator. *IEE Proc Pt C*, 137(2), 168-173.
5. Malik, N.H.; and Mazi, A.A. (1987). Capacitance requirements for isolated self excited induction generators. *IEEE Transactions on Energy Conversion*, 2(1), 62-69.
6. Al Jabri, A.K.; and Alolah, A.I. (1990). Capacitance requirement for isolated self-excited induction generators. *IEE Proc Pt B*, 137(3), 154-159.
7. Chan, T.F. (1993). Capacitance requirements of self-excited induction generators. *IEEE Transactions on Energy Conversion*, 8(2), 304-311.
8. Saied, M.M.; Hanafi, A.A.; El-Gabali, M.A.; Sharaf, A.M.; Safar, Y.A.; Jaboori, M.G.; and Yamin, K.H.A. (1991). Optimal design parameters for a PV array coupled to a dc motor via a dc-dc transformer. *IEEE Transactions on Energy Conversion*, 6(4), 593-598.
9. Alghuwainem, S.M. (1992). Steady-state performance of dc motors supplied from photovoltaic generators with a step-up converter. *IEEE Transactions on Energy Conversion*, 7(2), 267-272.
10. Alghuwainem, S.M. (1994). Matching of a DC motor to a photovoltaic generator using a step-up converter with a current-locked loop. *IEEE Transactions on Energy Conversion*, 9(1), 192-198.
11. Bansal, R.C. (2005). Three-phase self-excited induction generators: An overview. *IEEE Transactions on Energy Conversion*, 20(2), 292-299.
12. Ahmed, T.; Noro, O.; Matsuo, K.; Shindo Y.; and Nakaoka M. (2003). Minimum excitation capacitance requirements for wind turbine coupled stand-alone self-excited induction generator with voltage regulation based on SVC, *INTELEC'*03 *The* 25^{th} *International Telecommunications Energy Conference*, 396-403.
13. Al-Saffa, M.A.; Nho, E.C.; and Lipo T.A. (1998), Controlled shunt capacitor self-excited induction generator. In: *Proc. 33rd IEEE Industry Application. Soc. Annual Meeting,* 2, 1486-1490.
14. Bonert, R.; and Rajakaruna R. (1988). Self-excited induction generator with excellent voltage and frequency control. *IEE Proceedings*, *Generation*, *Transmission*, *and Distribution*, 145(1), 33-39.
15. Chan, T.F.; Nigim, K.A.; and Lai L.L. (2004). Voltage and frequency control of self-exited slip-ring induction generators. *IEEE Transactions on Energy Conversion*, 19(1), 81-87.

16. Chtchetninine, O. (1999). Voltage stabilization system for induction generator in stand alone mode. *IEEE Transactions on Energy Conversion* 14(3), 298-303.
17. Marra, E.G.; and Pamilio, J.A. (2000). Induction generator based system providing regulated voltage and constant frequency. *IEEE Trans Industrial Electronics*, 47(4), 908-914.
18. Saurez, E.; and Bortolotto, G. (1999). Voltage-frequency control of self-excited induction generator. *IEEE Transactions on Energy Conversion,* 14(3), 394-401.
19. Krause, P.C. (1987). *Analysis of Electric Machinery*, (1st Ed.). McGraw Hill, NY.
20. Akbaba, M. (2003). Matching 3-phase ac loads to PVG for maximum power transfer using enhanced version of Akbaba model and double step-up converter. *Solar Energy*, 75(1), 17-25.
21. Chapra, C.S.; and Canale, R.P. (2006). *Numerical methods for engineers*, (5th Ed.). McGraw Hill, NY.
22. Akbaba, M. (2006). Optimum matching parameters of an MPPT unit used for a PVG powered pumping system for maximum power transfer. *International Journal of Energy Research*, 30(6), 395-409.

Appendix A

Values of the parameters used for system components

DCM parameters:
R_a = 3.21 Ω,
L_a= 36 mH,
k_m = 0.485 V/rad/s,
J_{tot} = 0.0837 kgm^2, p_o = 1.

SEIG parameters other than magnetizing inductance:
240 V, 2 pole, 2 kW, 60 Hz,
Stator leakage inductance = rotor leakage inductance = 7.482 mH,
R_s = 2.046 Ω,
R_r = 2.051 Ω,
SEIG excitation capacitor (per phase) = 220 μF (or 114 μF in case of second load),

Chopper coil parameters:
L_{cp}= 4.6 mH,
R_{cp} =1.2 mΩ ,
dc-dc converter filter capacitors C_1=C_2=350 μF